Computer Physics Communications 63 (1991) 1–20
North-Holland

Time-dependent solution of the Liouville–von Neumann equation: non-dissipative evolution

Michael Berman and Ronnie Kosloff

Department of Physical Chemistry and The Fritz Haber Research Center for Molecular Dynamics, The Hebrew University, Jerusalem 91904, Israel

Received 18 December 1989

A method for solving the Liouville–von Neumann equation is presented. The action of operators is calculated locally in coordinate and/or momentum representation. The Fast Fourier Transform (FFT) is used to pass back and forth between coordinate and momentum representations, this transformation preserving all exact commutation relations. The time propagation is calculated by a Chebychev expansion of the time evolution operator. The accuracy and convergence properties of the method are investigated and compared with an exactly solvable model problem. Accurate converged results are obtained using a phase space boundary slightly exceeding the minimum theoretical value. Efficiency is attained by the natural vectorization options provided by the algorithm. A typical non-trivial application is presented, namely, the splitting up of the probability density of a non-pure state into transmitted and reflected branches due to scattering off a potential barrier.

1. Introduction

The Liouville–von Neumann equation is the basic framework unifying the quantum mechanical and statistical descriptions of matter. This framework is the only one permitting a consistent treatment of the transition from a pure state into a mixture. Such transitions are central in the description of the quantum mechanical measurement process [1] or in the decay of a system to thermal equilibrium [2].

This work presents a direct numerical solution of the Liouville–von Neumann equation. This means that realistic physical systems are amenable to exact treatment. Moreover, this solution may serve as a benchmark for various approximate methods.

In quantum statistical mechanics, the state of an ensemble of identical subsystems is completely specified by the density operator $\hat{\rho}$. Expectation values of an observable are fully determined by the relation: $\langle \hat{A} \rangle = \mathrm{tr}\{\hat{\rho}\hat{A}\}$. This statement constitutes the foundation of the axiomatic description of quantum mechanics [3,4] and the interpretation of measurement in quantum mechanical systems [1]. The density operator is the counterpart of the classical distribution function [5–7]. The same operator emerges from the quantum mechanical reduced description of open systems. In general, these systems cannot be described by wavefunctions [8,9]. The density operator is also the most convenient means of collecting all parameters of interest for an experimental set-up and of describing their behaviour [10].

Some physical examples in which the density operator has been utilized are sketched below *. The wealth of physical problems indicates the importance of having a general method for solving the time evolution of the density operator.

In the description of thermodynamic equilibrium, the density operator is time independent and assumes the canonical or grand canonical form. In these expressions the absolute temperature and the chemical potential of an ensemble in

* Only references not explicitly cited in ref. [9] are specified in the description of these examples.

0010-4655/91/$03.50 © 1991 – Elsevier Science Publishers B.V. (North-Holland)

thermodynamical equilibrium are naturally defined.

The density matrix has also been extensively used for many-body systems, such as atoms, molecules and nuclei. In the study of these systems, various techniques have emerged for systems at absolute zero temperature. In particular, mean-field techniques, such as Hartree–Fock and Thomas–Fermi approximations, have utilized reduced one-body density operators.

In solid state physics, both equilibrium and transport problems have been treated by means of the density operator. The diamagnetism of many-electron systems, such as conducting or semiconducting solids, is a typical example of equilibrium problems. Transport (non-equilibrium) processes, such as electrical conductivity, have received much attention in solid state physics. In these transport problems, the weak-coupling limit, for which the equilibrium density operator is a good approximating entity [11,12], has often been introduced.

It is worth mentioning the applications to polarization of light and angular correlation experiments. In the description of these experiments, the density operator is used to refer to only those degrees of freedom that are studied experimentally. A small number of relevant degrees of freedom is also characteristic of resonance and relaxation phenomena. For instance, the theory of masers and maser-like devices has been discussed in terms of the density operator. Other examples of relaxation phenomena include the absorption of microwave radiation in a gas and the Bloch nuclear induction equation. Vast applications in electron and nuclear magnetic resonances exist [13].

More recently, the density operator has been used for the description of atoms and molecules in strong electromagnetic fields [14]. Resonance fluorescence and resonance Raman obtained in the presence of intense fields have been described in the tetradic formalism.

The maximum entropy approach for systems not in equilibrium [15] has been used to define the density operator for a contracted set of relevant observables. Approximations to this approach have utilized algebraic methods [16] and variational techniques [17–19].

Time-dependent quantum mechanical methods have gained popularity in recent years. The advantage of such methods is the ability to monitor the dynamics instantaneously, resulting in physical insight. However, if only asymptotic results are desired, such a method may be expensive. In the framework of the time-dependent Schrödinger equation, appropriate for describing pure states, numerous studies have appeared. Only a few are mentioned here: (a) finite-difference techniques have been introduced to study reactive scattering [20,21], and electronic excitation [22]; (b) semi-classical time-dependent methods handling pure-state wave packets have found many applications [23,24]; (c) pseudo-spectral methods have been developed [25–27] and applied to molecular dynamics and surface scattering [28]; (d) the Lanczos algorithm has been utilized in the framework of time-dependent methods [29]. To summarize, time-dependent calculations of pure-state evolution have become established [30,31].

The propagation in time of the density operator is dictated by the Schrödinger picture Liouville–von Neumann equation of motion:

$$\frac{\partial \hat{\rho}}{\partial t} = -\mathrm{i} L \hat{\rho}, \tag{1.1}$$

where L is the differential superoperator; atomic units are used throughout the text, which implies $\hbar = 1$. The formal solution of this equation for a time-independent L reads:

$$\hat{\rho}(t) = U(t)\hat{\rho}(0) = \mathrm{e}^{-\mathrm{i}Lt}\rho(0), \tag{1.2}$$

where U is the time evolution superoperator.

The form of L depends on the properties of the system considered. For an isolated (closed) physical system, the time evolution is reversible. This implies that the variation in time is determined by a unitary dynamical group, i.e. U is unitary. As is well known [1,32], for a unitary evolution L is given by

$$L_{\mathrm{H}}\hat{\rho} = \left[\hat{H}, \hat{\rho}\right], \tag{1.3}$$

where $\hat{H}$ is the Hamiltonian operator of the system. Open quantum mechanical systems, however, exhibit irreversible behaviour with respect to time evolution, such behaviour being a consequence of the interaction with the external world. To obtain

equations of motion for the open system alone, a reduced description of the dynamics is required [9,32]. A basic ingredient of the reduction procedure is the assumption that the total evolution of the system and its environment is Hamiltonian (unitary). A direct consequence of this assumption is that the reduced dynamics follows an evolution law corresponding to a completely positive semi-group [33,34]. A differential description of the equation of motion (1.1) for open systems is equivalent to no preservation of past events for future evolution (no memory). Lindblad [33] has shown that a completely positive semi-group evolution, together with the "no memory" assumption leads to completely dissipative dynamics. Moreover, he derives the structure of the Liouville differential superoperator

$$-\mathrm{i}L_{\mathrm{D}}\hat{\rho} = \tfrac{1}{2}\sum_j \left(\left[\hat{W}_j\hat{\rho},\ \hat{W}_j^{\dagger} \right] + \left[\hat{W}_j,\ \hat{\rho}\hat{W}_j^{\dagger} \right] \right), \quad (1.4)$$

where $\hat{W}_j$ are operators from the Hilbert space of the open system being considered. Special solvable examples such as the weak-coupling limit [32,35] and the singular bath case [36,37] in which the reduced dynamics is solved explicitly, exhibit the form of eq. (1.4). The dissipative character of open systems dictates a more involved solution of the equation of motion (1.1). Thus to keep the argument clear, a detailed description of open systems is postponed [38].

As stated previously, we are aiming at a direct numerical solution of the Liouville–von Neumann equation (1.1). The following requirements should be fulfilled by the numerical approach: (i) The solution should be general and flexible. This means that various physical systems may be handled and potentials, masses and other physical parameters may be changed with ease. (ii) The solution should be numerically accurate. Convergence of the numerical method should be fast. (iii) The algorithm should be efficient. Efficiency permits the simulation of realistic physical systems.

As far as we know, no direct numerical method for the solution of the Liouville–von Neumann equation (1.1) has been attempted. This is a consequence of the inherent difficulties of quantum mechanical equations in general and the superoperator structure of the Liouville equation in particular. Quantum mechanical equations of motion are difficult to solve due to: (a) The need for a simultaneous global description of space and momentum. This numerical effort scales with the volume of phase space needed to describe the system, divided by h. (b) The quantum equations of motion involve operators as opposed to scalars in classical mechanics, the non-commutative nature of these operators complicating the solution. (c) Characteristic time scales of the propagation are limited by the maximum energy accommodated in the system according to the time–energy uncertainty principle. This is in contradistinction to the local relations found in classical mechanics. In addition to these difficulties, the Liouville–von Neumann equation (1.1) poses further problems. These include a double dimensionality of the equation of motion as compared with the time-dependent Schrödinger equation, as well as a more complicated differential superoperator. Despite the above difficulties, quantum mechanical equations of motion are linear. This fact is exploited to the utmost in the solution presented in this work.

It is desirable that a numerical algorithm chosen to solve the Liouville–von Neumann equation preserve the commutation relations as well as the time–energy uncertainty relation. It is clear from eqs. (1.3), (1.4) that the commutation relations play a central role. The discretization method presented in this work maintains the correct commutation relations in the discrete world. Moreover, the propagation scheme preserves the time–energy uncertainty principle.

In our algorithm, the discretization of the Hilbert space is done by a pseudospectral (or collocation) method. In this scheme the approximated entity matches the true value on a set of discrete points, while values in between points are obtained by interpolation. Usually, the Liouville superoperator is constructed out of local operators in coordinate representation, e.g. the potential operator, and non-local ones such as the kinetic energy operator. However, the kinetic energy operator is local in momentum representation. In the discrete world used in this work, all operator actions as well as commutation relations are calculated locally. The transformation from coor-

dinate to momentum representation is achieved by discrete Fast Fourier Transform (FFT) [39] algorithm. This transformation maintains the basic commutation relation of position and momentum in the discrete world [40]. Thus, all commutation relations in eqs. (1.1)–(1.4) are preserved. Moreover, the use of the FFT device is the source of the numerical efficiency of the method. The FFT is ideally suited to vector and parallel processing incorporated in modern computers [41–43].

The time propagation of the density operator is carried out by a truncated polynomial expansion of the evolution superoperator:

$$e^{-iLt} = \sum a_n P_n(-iLt), \tag{1.5}$$

where a_n are the expansion coefficients and P_n are polynomials of degree n. This expansion exploits the fact that L is a linear time-independent superoperator. For a Hamiltonian conservative evolution (unitary $\hat{U}$), the eigenvalues of L are real. For the time-dependent Schrödinger equation, a Chebychev polynomial expansion of the evolution operator has shown exponential convergence. This property carries over to the non-dissipative Liouville superoperator in eq. (1.3). For the dissipative evolution for which the eigenvalues of L are complex, a different polynomial expansion has been devised and will be presented elsewhere [38]. The desired flexibility of a numerical approach is naturally acquired by the method, as the discretization scheme allows an easy replacement of potentials, masses and other physical parameters. The combination of the Fourier representation of Hilbert space and the polynomial expansion of the time propagation superoperator results in an exponentially convergent scheme for the solution of the Liouville–von Neumann equation.

In order to check the method a few pilot analytically solvable cases have been studied. The solutions of these serve to check the predicted convergence and efficiency of the algorithm. In addition, they guarantee the technical correctness of the numerical codes. The analytical examples chosen have been solved by an algebraic method adopted from the work of Alhassid and Levine [16].

Once the numerical algorithm is checked, its relation to analytic solutions is reversed. The numerical solution can be used to check analytic approximations. Recently the local harmonic approximation for the Landau–Teller case, as well as a variational self-consistent approximation [44] have been developed. The method evolved here is almost the only way of checking the validity of these approximations.

2. Theoretical considerations

The physical and mathematical properties of the density operator and the Liouville–von Neumann equation have a direct influence on the structure of the method. Therefore, a survey of these properties and their relation to physical and mathematical concepts encountered in this work, is presented.

The properties of the density operator $\hat{\rho}$ follow from its physical interpretation as the analog of the classical probability density. According to this interpretation, the eigenvalues are probabilities meaning that $\hat{\rho}$ is Hermitian, positive definite and normalized to one:

$$\mathrm{tr}\{\hat{\rho}\} = 1. \tag{2.1}$$

Moreover,

$$\mathrm{tr}\{\hat{\rho}^2\} \leqslant 1. \tag{2.2}$$

A dispersion-free density operator is called a pure state. For such a state only one eigenvalue is different from zero, which corresponds to the equality in eq. (2.2). A mixed state corresponds to the inequality in (2.2), equivalently the entropy $S = -\mathrm{tr}\{\hat{\rho} \log \hat{\rho}\}$ is positive. The inequality (2.2) imposes a limitation on all elements of the density operator in any representation.

In this work, two equivalent representations are utilized for the description of $\hat{\rho}$, namely those of the free particle in coordinate and momentum space:

$$\begin{aligned} \rho(x, x') &= \langle x | \hat{\rho} | x' \rangle, \\ \rho(k, k') &= \langle k | \hat{\rho} | k' \rangle. \end{aligned} \tag{2.3}$$

The transformation from x- to k-space is defined by the free-particle plane waves:

$$\langle x \mid k \rangle = \frac{1}{\sqrt{2\pi}} \, \mathrm{e}^{\mathrm{i}kx}. \tag{2.4}$$

From eq. (2.4) the transformation from coordinate space to momentum space of the density operator becomes:

$$\rho(k, k') = \int\int \langle k \mid x \rangle \langle x \mid \hat{\rho} \mid x' \rangle \langle x' \mid k' \rangle \, \mathrm{d}x \, \mathrm{d}x', \tag{2.5}$$

or:

$$\rho(k, k') = \frac{1}{2\pi} \int\int \mathrm{d}x \, \mathrm{d}x' \, \mathrm{e}^{-\mathrm{i}kx} \rho(x, x') \, \mathrm{e}^{\mathrm{i}k'x'}.$$

Equation (2.5) is recognized as a combination of a forward and a backward Fourier transform. The inverse transformation from momentum to coordinate space has a similar form:

$$\rho(x, x') = \int\int \langle x \mid k \rangle \langle k \mid \hat{\rho} \mid k' \rangle \langle k' \mid x' \rangle \, \mathrm{d}k \, \mathrm{d}k',$$

$$\rho(x, x') = \frac{1}{2\pi} \int\int \mathrm{d}k \, \mathrm{d}k' \, \mathrm{e}^{\mathrm{i}kx} \rho(k, k') \, \mathrm{e}^{-\mathrm{i}k'x'}. \tag{2.6}$$

The transformations presented in eqs. (2.5) and (2.6) are at the heart of the method presented here. These transformations permit the *local* calculations of the operator commutation relations.

Periodic boundary conditions in coordinate space are imposed on the underlying Hilbert space. In addition, a cutoff in momentum space is introduced, equivalent to a limit on the maximum kinetic energy. As a consquence of the uncertainty principle, the cutoff in momentum and the periodic boundary conditions imply a discretized representation in coordinate space with a grid displacement defined by $\Delta x k_{\max} = \pi$. Mathematically this physically motivated discretization scheme is equivalent to a pseudo-spectral collocation method [45]. In the pseudo-spectral method a function $u(x)$ in Hilbert space is represented by a truncated series

$$u_N(x) = \sum_{i=0}^{N-1} a_i \eta_i(x) \tag{2.7}$$

in known functions η, where N is the number of collocation points. In the collocation method the approximate function $u_N(x)$ coincides with the exact function $u(x)$ at a set of discrete sampling points $x_0, x_1, \ldots, x_{N-1}$.

$$u_N(x_j) = u(x_j), \quad j = 0, \ldots, N-1. \tag{2.8}$$

This matching determines the expansion coefficients a_i. The solution at other points is obtained by interpolation. The choice of the free-particle plane waves in eq. (2.4) is translated in the discrete representation into

$$\eta_k(x) = \mathrm{e}^{2\pi \mathrm{i} x k},$$

$$k = -(N/2-1), \ldots, 0, \ldots, N/2, \tag{2.9}$$

where here k is the discrete momentum as well as the expansion index in eq. (2.9). The coefficients a_k are determined by the discrete Fourier transform. For equidistant sampling points these coefficients read:

$$a_k = \frac{1}{N} \sum_{j=-(N/2-1)}^{N/2} u(x_j) \, \mathrm{e}^{-2\pi x_j k}. \tag{2.10}$$

This choice of expansion is called the Fourier method.

The functions encountered in quantum mechanics are approximately band-limited and are semilocal (having nearly finite support) [45]. Gaussian functions, appearing in many physical situations such as in coherent states or in semiclassical methods, constitute a well-known example of these functions. The Whittaker–Kotel'nikov–Shannon sampling theorem [46–49] states that a band-limited function is fully specified if the function values are given at a discrete, sufficiently dense set of equally spaced sampling points. This implies that the value at a point between the sampling points can be interpolated with any desired accuracy. An important consequence of the sampling theorem is exponential convergence in the approximation of functions encountered in quantum mechanics [46].

In the Fourier discretization scheme $\hat{\rho}$ is represented as:

$$\hat{\rho}(x, x') \equiv \{\rho_{ij}\} \equiv \begin{bmatrix} \rho_{00} & \rho_{01} & \cdot & \cdot \\ \rho_{10} & \rho_{11} & \cdot & \cdot \\ \cdot & \cdot & \cdot & \cdot \\ \cdot & \cdot & \cdot & \cdot \end{bmatrix},$$
$$x = i\Delta x, \quad x' = j\Delta x. \tag{2.11}$$

Dealing with a finite matrix representation of $\hat{\rho}$ there are altogether N^2 complex matrix elements ρ_{ij}, that is $2N^2$ parameters. This number is reduced by a factor of 2 because of the Hermiticity of $\hat{\rho}$ and reduced by 1 because of the normalization condition (2.2), so that there are $N^2 - 1$ independent parameters [9,10]. Expectation values of observables in this discrete world are obtained by:

$$\langle \hat{A} \rangle = \mathrm{tr}\{\hat{\rho}\hat{A}\}, \tag{2.12}$$

where $\hat{\rho}\hat{A}$ is the matrix product of the operators in the discrete representation.

Dealing specifically with the unitary Liouville superoperator (1.3), one notes that all eigenvalues of L are real. These eigenvalues correspond to energy differences, to the exclusion of unobservable absolute energies appearing in the Schrödinger equation. As is clear from eq. (1.3) the operation of L implies the use of a commutator with the Hamiltonian $\hat{H}$:

$$\hat{H} = \hat{K} + \hat{V}(x), \tag{2.13}$$

where $\hat{K}$ is the kinetic energy operator and $\hat{V}$ is the potential energy operator. The potential operator is diagonal in coordinate space:

$$V(x, x') = \langle x | \hat{V} | x' \rangle = V(x)\delta(x - x'). \tag{2.14}$$

Therefore, a discrete coordinate representation is appropriate for the potential operator:

$$\hat{V}(x, x') \equiv \{V_i \delta_{ij}\} \equiv \begin{bmatrix} V_0 & 0 & \cdot & \cdot \\ 0 & V_1 & \cdot & \cdot \\ \cdot & \cdot & \cdot & \cdot \\ \cdot & \cdot & \cdot & \cdot \end{bmatrix}, \tag{2.15}$$

while the kinetic energy operator is diagonal in k-space:

$$\tilde{K}(k, k') = \langle k | (k^2/2m) | k' \rangle = (k^2/2m)\delta(k - k') \tag{2.16}$$

having the discrete representation:

$$\tilde{K}(k, k') \equiv \left\{ \frac{k_i^2}{2m} \delta_{ij} \right\} \equiv \begin{bmatrix} k_0^2/2m & 0 & \cdot & \cdot \\ 0 & k_1^2/2m & \cdot & \cdot \\ \cdot & \cdot & \cdot & \cdot \\ \cdot & \cdot & \cdot & \cdot \end{bmatrix}. \tag{2.17}$$

In the discrete representations the communication relations inherent in the Liouville superoperator are calculated in the following way. For the potential part:

$$[\hat{V}, \hat{\rho}] = \hat{V}\hat{\rho} - \hat{\rho}\hat{V}, \tag{2.18}$$

$$(V\rho)_{ij} = \sum_k V_{ik}\rho_{kj} = \sum_k V_i \delta_{ik}\rho_{kj} = V_i \rho_{ij}, \tag{2.19}$$

$$(\rho V)_{ij} = \sum_k \rho_{ik} V_{kj} = \sum_k \rho_{ik} V_k \delta_{kj} = \rho_{ij} V_j,$$

which leads to:

$$([\hat{V}, \hat{\rho}])_{ij} = V_i \rho_{ij} - \rho_{ij} V_j = (V_i - V_j)\rho_{ij}. \tag{2.20}$$

Commutation relations in momentum space for the kinetic energy operator take the local form:

$$([\tilde{K}, \tilde{\rho}])_{ij} = (\tilde{K}\tilde{\rho} - \tilde{\rho}\tilde{K})_{ij} = \frac{1}{2m}(k_i^2 - k_j^2)\tilde{\rho}_{ij}, \tag{2.21}$$

where $\tilde{O}$ designates the Fourier-transformed operator (coordinate to momentum), which is also the momentum representation of the operator. Clearly $[\hat{V}, \hat{\rho}]$ and $[\hat{K}, \hat{\rho}]$ are traceless.

The variation in time of observables follows from the time dependence of the density operator in the Schrödinger picture as shown in eq. (2.12). The Liouville–von Neumann equation (1.1) dictates the time evolution of $\hat{\rho}(t)$. For a unitary evolution $L_H = -\mathrm{i}[H,]$, not only is the trace of $\hat{\rho}$ preserved in time, but the trace of any analytic function of $\hat{\rho}$ is conserved as well. Specifically, $\mathrm{tr}\{\hat{\rho}^2\} = \text{constant}$ and the entropy $S = -\mathrm{tr}\{\hat{\rho} \ln \hat{\rho}\}$ is constant. The conservation of both these functions indicates that no dissipation may occur in the unitary evolution [1]. This property is routinely used as a cross check on the results. The mathematical definition of the formal solution

(1.2) for $\hat{\rho}(t)$ contains a power series in $-\mathrm{i}Lt$. The existence of this expansion relies on L being a bound superoperator, i.e. all its eigenvalues are finite. It follows from the Campbell–Baker–Hausdorff formula [50] and the existence of the power expansion, that for time-independent Hamiltonians $\rho(t) = \mathrm{e}^{-\mathrm{i}\hat{H}t}\rho(0)\mathrm{e}^{\mathrm{i}\hat{H}t}$. The invariance in time of the trace of analytic functions of $\hat{\rho}$ for unitary evolution follows directly from this last relation.

A truncated Taylor expansion of $U(t) = \mathrm{e}^{-\mathrm{i}Lt}$ could be used, in principle, to propagate $\hat{\rho}$. However, the Taylor series expansion converges fastest near the origin. The range of the eigenvalues of the superoperator $-\mathrm{i}Lt$ is spanned on the imaginary axis far from the origin. As the propagation proceeds, increasing t, this range is linearly extended. Consequently, a uniformly convergent series expansion is needed. The situation is analogous to the polynomial expansion of the function $\mathrm{e}^{\mathrm{i}x}$, for which the Chebychev polynomial is best suited, i.e. out of all possible polynomial expansions the maximum error is minimal for the Chebychev one [51]. Using the Chebychev expansion the approximate evolution operator (eq. (1.5)) reads:

$$\mathrm{e}^{-\mathrm{i}Lt} \approx \sum_{n=0}^{M} a_n \phi_n(-\mathrm{i}Lt/R), \tag{2.22}$$

where: $a_n = 2J_n(R)$ for $n \neq 0$ and $a_0 = J_0(R)$, J_n being the Bessel function of the first kind and R being the area in energy–time phase space describing the evolution of the system. R is estimated as the product of time by the upper bound of the range of eigenvalues of L (represented on the grid):

$$R = \left(V_{\max} - V_{\min} + k^2_{\max}/2m\right)t \tag{2.23}$$

(for a one-dimensional grid). The radius of convergence R in (2.23) determines the effective number M of Chebychev polynomials in (2.22), the reason being that the Bessel expansion coefficients a_n decay exponentially when their order n is larger than their argument R [52]. ϕ_n are the complex Chebychev polynomials calculated by their recursion relation:

$$\phi_n(\hat{X}) = 2\phi_{n-1}(\hat{X})\hat{X} + \phi_{n-2}(\hat{X}), \tag{2.24}$$

where $\hat{X} = -\mathrm{i}Lt/R$, $\phi_0(\hat{X}) = \hat{I}$ and $\phi_1(\hat{X}) = \hat{X}$. A similar approach has been used for the Schrödinger equation [53,54].

3. Development of the basic algorithm

The present section is intended as a comprehensive description of the algorithm. The method has a modular structure well suited for parallel and vector computing, which guaranties flexibility in the choice of physical systems. At the heart of the algorithm is the calculation of the action of the Liouville superoperator L, this operation being performed repeatedly for each time step. As this action is rate-determining, it should be performed with the utmost efficiency. The Liouville superoperator should work on operators with the dimensions of $\hat{\rho}$. The representation of these operators may result in very large matrices. However, the design of the algorithm minimizes the number of such operators needed for the propagation, thus reducing storage requirements. The algorithm is divided into the following steps:

A. Initiation:
[A.1] Discretizing the Hilbert space of the system.
[A.2] Initiation of the time propagation.
[A.3] Preparing an initial density operator.
B. Propagation cycle:
[B.1] The operation of the Liouville superoperator.
[B.2] Propagating in time.
[B.3] Analyzing intermediate results.
C. Final analysis.

A. Initiation

The initiation step consists of preparing the modules needed for the time propagation cycle. The physical properties of the system dictate the initialization procedures. The relevant physical parameters are the geometrical size of the system, the maximum of the momentum allowed, the range of kinetic and potential energy and the time step in which the system is monitored. However, these parameters may be updated according to the intermediate results of the propagation cycle.

[A.1] Discretizing the Hilbert space of the system

The geometry of the configuration space is first determined by the range of the potential in each degree of freedom. As will become clear later, reducing the dimensionality using symmetry considerations is very beneficial, the numerical effort being crucially dependent on the dimensionality of the problem. The initial density operator should be contained in the range of configuration space. Moreover, this should also be true for the propagated density operator which should not extend over the boundary of configuration space. If a situation occurs in which the density operator evolves over this edge, the range of configuration space may be dynamically updated.

In order to deal with a finite phase space, a cutoff in momentum has to be introduced, the value of this cutoff depending on the initial spread of momentum for the process and the maximum momentum transfer induced by the potential. Once the size of configuration space l and the momentum cutoff $p_{\max}$ are fixed in each degree of freedom, the total volume of phase space is given according to:

$$\text{Volume} = (\boldsymbol{l} \cdot \boldsymbol{p}_{\max}), \tag{3.1}$$

where $\boldsymbol{l}$ and $\boldsymbol{p}_{\max}$, respectively, are the vectors of range values and momentum cutoffs in each degree of freedom. The discretization scheme of phase space is a consequence of the usage of the FFT algorithm, which imposes periodic boundary conditions on configuration space and equidistant sampling of phase space. The sampling spacing is related to the maximum momentum (in one dimension) via:

$$\Delta x = \frac{\pi}{k_{\max}}. \tag{3.2a}$$

The number of sampling points N is obviously $l/\Delta x$. Using eqs. (3.1) and (3.2):

$$N = \frac{l}{\Delta x} = \frac{l k_{\max}}{\pi} = \frac{\text{Volume}}{h}, \tag{3.2b}$$

where h is the Planck's constant. This is in accord with the well-known statistical mechanics result stating that the size of a cell in quantum mechanical phase space is h. In practice, the accuracy of the method is controlled by the volume of phase space and by increasing this volume (increasing N), convergence can be checked. As stated in the theoretical description and demonstrated in the examples, the convergence with N is exponential [45].

On this discrete Hilbert space, operators such as the density operator $\hat{\rho}$, are represented as matrices. As explained under eq. (2.11) the number of independent parameters for Hermitian operators on this Hilbert space is N^2, the Hermitian property permitting a reduction of storage by a factor of two. Local operators in either coordinate or momentum representations are diagonal and therefore have only N independent parameters, examples of such local operators being the kinetic and potential energy. Once the discretization is set, these operators are constructed and stored for use in the propagation cycle.

In considering realistic problems, the density operator may propagate towards the edge of the finite phase space so that an obvious solution would be to increase the size of the phase space. Usually, the repulsive part of the potential prevents the operator $\hat{\rho}$ from reaching the boundary, but beyond the repulsive wall, the classically forbidden region, the density operator diminishes exponentially. The end of the grid should be chosen such that this exponential tail is smaller than the desired accuracy. Extending phase space further in the repulsive region would be wasteful. A semiclassical estimate of the extent of tunneling can guide the placing of the end of the grid. An alternative option is to introduce a physically unimportant cut on the repulsive wing of the potential, this cut reducing the range of eigenvalues of the Liouville superoperator. This, in turn, decreases the numerical effort for the propagation cycle as described below and to compensate for this cut, the size of the forbidden region has to be increased. These two contradicting tendencies should be optimized.

[A.2] Initiation of the time propagation

For each physical system a characteristic time scale exists, the total propagation time being estimated with regard to this time scale. Examples of such natural time scales are the lifetime of a target in a scattering experiment, a period of an

oscillator, and the mean passage time in the experimental setup. Often, much information is gained by inspecting the dynamics at intermediate time steps which refer to the time step t in eq. (2.22) used in the propagation cycle. Equations (2.22)–(2.24) define the propagation method. At the initiation stage, the radius of convergence R [cf. eq. (2.23)] is calculated. R may also be interpreted as the volume of the time–energy "phase space". The maximum and minimum of the kinetic and potential energy determining R have been calculated in module [A.1]. Furthermore, the volume in the time–energy "phase space" determines the effective number M of Chebychev polynomials via

$$M \geqslant R/\hbar. \tag{3.3}$$

In practice, the expansion coefficients a_n, which are up to a factor Bessel functions $J_n(R)$, are calculated for all $n \leqslant M$. The last coefficient a_M has to be smaller than the predetermined accuracy criterion of the calculation. The larger the volume R, the closer M is to the theoretical value, cf. eq. (3.3). The reason for this is that the Bessel expansion coefficients a_n decay exponentially when their order n is larger than their argument R [52]. Thus, for each R there is a "tail" of coefficients needed for convergence. The desire for efficiency imposes the usage of long time steps as the number of "tails" used in the course of the propagation cycle is reduced. Therefore, an inspection of intermediate time steps is expensive.

Despite the aforementioned considerations as to the duration of the time step, expectation values of observables $\langle \hat{O} \rangle$ may be monitored at a finer time scale without a significant increase in the numerical effort. It follows from eq. (2.22) that:

$$\begin{aligned}\langle \hat{O} \rangle(t) &= \mathrm{tr}\{\hat{O}\hat{\rho}(t)\} \\ &= \sum_n a_n \mathrm{tr}\{\hat{O}\phi_n(-\mathrm{i}L/\Delta E)\hat{\rho}(0)\},\end{aligned} \tag{3.4}$$

where $\Delta E = V_{\max} - V_{\min} + k^2_{\max}/2m$ is the range of energy. The explicit calculation of the superoperation of Chebychev polynomials $\phi_n(-\mathrm{i}L/\Delta E)$ is described in modules [B.2] and [B.3] below. Note that the traces on the rhs of eq. (3.4) are time-independent. Therefore, the calculation of these traces is done only once and stored for usage with expansion coefficients a_n for a variety of intermediate times. The trace operation results in a number; thus, the storage requirement is negligible. The coefficients a_n and ΔE are calculated at the initiation module for later use in the propagation cycle [B.2] and [B.3].

[A.3] Preparing an initial density operator

Pure initial density operators may be constructed from their corresponding wavefunction via:

$$\rho(x, x') = \psi(x)\psi^*(x'). \tag{3.5}$$

A discretization of ψ on the grid, which is an eigenfunction of $\hat{H}$ as defined in module [A.1], may be constructed as in ref. [54]. For unitary evolution the pure state is of interest only for technical checks. The relaxation of a pure state is studied in a future paper [38].

Thermal initial states can be constructed by a Bolzmann weighting of energy eigenstates. For a few cases, e.g. the harmonic oscillator [55], this weighting procedure may be obtained in closed form.

Most initial states used in this work are of a Gaussian type. A Gaussian density operator is determined explicitly by the set of expectation values: $\langle \hat{x} \rangle$, $\langle \hat{p} \rangle$, $\langle \hat{x}^2 \rangle$, $\langle \hat{x}\hat{p} + \hat{p}\hat{x} \rangle$ and $\langle \hat{p}^2 \rangle$. The most general one-dimensional Gaussian density operator has the form:

$$\begin{aligned}\rho(x, x', t=0) &= \langle x \,|\, \hat{\rho} \,|\, x' \rangle \\ &= \langle x \,|\, \exp\big(\lambda_0 + \lambda_1 \hat{x} + \lambda_2 \hat{p} + \lambda_3 \hat{x}^2 \\ &\quad + \lambda_4 1/2(\hat{x}\hat{p} + \hat{p}\hat{x}) + \lambda_5 \hat{p}^2\big) \,|\, x' \rangle,\end{aligned} \tag{3.6}$$

where λ_i are the Lagrange coefficients. In the appendix the relations between the Lagrange coefficients and the expectation values are displayed.

For an initial coherent state [55] which is a pure Gaussian state a simpler expression exists [56]:

$$\rho(x, x', t=0) = \left[\frac{2\alpha_1}{\pi}\right]^{1/2} \exp\Big\{-\alpha_1\big[(x-\langle\hat{x}\rangle)^2 + (x'-\langle\hat{x}\rangle)^2\big] + i\alpha_2\big[(x-\langle\hat{x}\rangle)^2 - (x'-\langle\hat{x}\rangle)^2\big] + i\langle\hat{p}\rangle(x-x')\Big\}. \quad (3.7)$$

Gaussian initial density operators have been used in the examples studied in this work.

B. Propagation cycle

The propagation cycle constitutes the time-consuming stage of the algorithm. Therefore, investment in optimizing this module is most beneficial. Advantage can be taken of modern parallel and vector computing, as the FFT algorithm may be peformed in a parallel architecture [41–43]. In addition, the matrix and vector representations of the operators enable vector processing.

[B.1] The operation of the Liouville superoperator

The unitary Liouville superoperator action is defined in eq. (1.3) whereas in the discrete representation this action is performed according to eqs. (2.20), (2.21). The local calculation of the kinetic energy commutation relation, eq. (2.21), requires a mixed forward and backward discrete Fourier transform:

$$\tilde{O}(k_j, k_l') = \frac{1}{2\pi N}\sum_{m=0}^{N-1}\sum_{n=0}^{N-1}\hat{O}(x_m, x_n') \times \exp[2\pi i(-jm/N + ln/N)], \quad (3.8)$$

for $j = 0, 1, \ldots N-1$ and $l = 0, 1, \ldots n-1$, which is the discretized version of eq. (2.5). A similar equation results for the discrete analog of eq. (2.6). In practice, eq. (3.8) is performed according to the mixed Radix FFT algorithm of Temperton [57]. This method efficiently handles the non-consecutive elements met in the backward–forward FFT.

The Liouville action is performed repeatedly as will be seen in [B.2] below. The sequence of operations to achieve this action on a given operator $\hat{O}(x, x')$ is as follows: (i) Perform an FFT transformation (3.8) on $\hat{O}$ and obtain $\tilde{O}$. (ii) Multiply $(\tilde{O})_{ij}$ by $(1/2m)\,(k_i^2 - k_j^2)$ for all i and j. (iii) Back transform the result according to the inverse of eq. (3.8). (iv) Multiply $(\hat{O})_{ij}$ by $V_j - V_i$ for all i and j [as in eq. (2.20)] and add the result to the result of step (iii) to complete the Liouville action.

[B.2] Propagating in time

The time propagation consists of two main parts namely, the accumulation equation (2.22) and the recursion relation (2.24) of the Chebychev polynomials. For each n in eq. (2.24), the Chebychev polynomial of order n is calculated recursively using the Liouville action of [B.1] above. The propagated density operator is updated by accumulating the recursive result multiplied by a_n into its current matrix representation. The recurrence relation requires temporary storage matrices.

This procedure is repeated for all time steps until the total propagation time is reached.

[B.3] Analyzing intermediate results

As the density operator contains all dynamical information on the system, the time dependence of any observable of interest may be followed. Using eq. (3.4) expectation values of dynamical observables are accumulated. Dynamical information requiring significant storage, e.g. the Wigner distribution function, is calculated only at the end of each time interval and not at the finer time scales.

Conserved quantities such as the energy $\mathrm{tr}\{\hat{\rho}\hat{H}\}$ and the norm $\mathrm{tr}\{\rho\}$ are calculated at each time step as a check on the accuracy of the propagation. The unitary property of the evolution is also checked by calculating $\mathrm{tr}\{\hat{\rho}^2\}$ as discussed in the theoretical considerations, section 2.

C. Final analysis

At this stage asymptotic values of the quantities analyzed in each time step are gathered. Care should be taken to assure that the collision has been completed.

4. The harmonic oscillator: comparing numerical with analytical results

The solutions of the Liouville–von Neumann equation (1.1), (1.3) for the harmonic oscillator are known in closed form and are used to illustrate the convergence properties of the algorithm. The numerical procedure makes no use of the properties of the harmonic oscillator. A Gaussian initial density operator is propagated numerically and compared with its analytical counterpart. In addition, observables calculated according to eq. (3.4) are checked against their analytic value, the purpose of these comparisons being to confirm the theoretical claims made in section 2 on the accuracy of the numerical procedure.

A convenient presentation of the closed-form solution to the harmonic oscillator is in terms of an algebraic formulation [58,16]. The dynamical algebra of the operators $\hat{I}$, $\hat{x}$, $\hat{p}$, may serve to define and propagate the density operator. This algebra, together with its first enveloping field, has been used to define the initial Gaussian density operator (3.6). The Gaussian form of this state is maintained in the course of the time evolution of the harmonic oscillator. This is a manifestation of the algebraic structure

$$[\hat{H}, \hat{Z}_i] = \sum_{j=0}^{2} \beta_{ij} \hat{Z}_j, \tag{4.1}$$

where $\hat{H}$ is the Hamiltonian of the harmonic oscillator, $\{\hat{Z}_i\}$ are $\hat{I}$, $\hat{x}$, $\hat{p}$, and

$$\beta_{12} = -\mathrm{i}/m, \qquad \beta_{21} = \mathrm{i}m\omega^2. \tag{4.2}$$

The density operator at time t has the functional form (3.6) with the Lagrange coefficients λ_i dependent on time. The explicit time dependence of the dynamical observables generating the algebra is given by [16,44]

$$\langle \tilde{Z} \rangle_t = \exp\left(\frac{-1}{\mathrm{i}} \tilde{\beta} t\right) \langle \tilde{Z} \rangle_0 = \tilde{b} \langle \tilde{Z} \rangle_0, \tag{4.3}$$

$$\langle \tilde{Z} \otimes \tilde{Z} \rangle_t = \tilde{b} \otimes \tilde{b} \langle \tilde{Z} \otimes \tilde{Z} \rangle_0,$$

where the $\otimes$ denotes the direct product [59]. The Lagrange coefficients λ evolve contra-gradiently to the expectation values in eq. (4.3) [16].

For the pure-state case, the algebraic form of the density operator (3.6) becomes singular and the simpler form (3.7) is appropriate. The evolution in time of this pure state is determined by the equations [60]

$$\langle x \rangle_t = \langle x \rangle_0 \cos \omega t + \frac{\langle p \rangle_0}{m\omega} \sin \omega t, \tag{4.4}$$

$$\langle p \rangle_t = \langle p \rangle_0 \cos \omega t - \langle x \rangle_0 m\omega \sin \omega t,$$

and for the width parameters [61]

$$\alpha_t = -\frac{m\omega}{2} \left[\frac{\frac{1}{2}m\omega - \alpha_0 \cot(\omega t)}{\alpha_0 + \frac{1}{2}m\omega \cot(\omega t)} \right]. \tag{4.5}$$

The connection between α and the expectation values is given by the relation:

$$\mathrm{Im}\ \alpha = \frac{0.25}{\langle x^2 \rangle - \langle x \rangle^2} \tag{4.6}$$

and

$$\mathrm{Re}\ \alpha = \left[\mathrm{Im}\ \alpha \left(\langle p^2 \rangle - \langle p \rangle^2 \right) - (\mathrm{Im}\ \alpha)^2 \right]^{1/2}.$$

Discretizing the phase space is the starting point of the algorithm. In order to check the convergence of this representation, the Liouville equation has been solved with various discretization boxes in phase space. The frequency and mass of the oscillator has been chosen to simulate the hydrogen molecule. A mixed Gaussian initial state corresponding to eq. (3.6) has been used in all tested cases. Table 1 summarizes the physical parameters of the oscillator and the initial conditions. In order to monitor the convergence in coordinate–momentum phase space only, the propagation in time has been performed with the highest accu-

Table 1
Physical parameters and initial conditions of the oscillator

Physical parameters	
mass	911.5 a.u.
ω	0.02 a.u.
Initial conditions	
$\langle x(0) \rangle$	0. a.u.
$\langle p(0) \rangle$	1. a.u.
$\langle x^2(0) \rangle$	0.1 a.u.
$\langle \frac{1}{2}(xp(0) + px(0)) \rangle$	0. a.u.
$\langle p^2(0) \rangle$	5. a.u.

racy. Table 2(a) shows the convergence of the method with respect to extending phase space in the momentum direction. This has been done by keeping the grid length $l = 4$ a.u. constant while varying the maximum momentum. The oscillator has been propagated for one cycle, meaning that all expectation values have to return to their initial value. The last column in table 2 depicts the

Table 2(a)
Convergence of the method with respect to extending phase space in the momentum direction

N	5	8	10	16	20	32	40	
Δx	0.8	0.5	0.4	0.25	0.2	0.125	0.1	
l	4	4	4	4	4	4	4	analytical
$p_{\max}$	1.25π	2π	1.5π	4π	6π	8π	10π	
$\mathrm{tr}\{\rho(0)\}$	0.908480	1.00074	1.0001	1.	1.	1.	0.999997	1.
$\mathrm{tr}\{\rho(1)\}$	0.908478	1.00074	1.0001	0.999997	0.999997	0.999997	0.999997	1.
$\langle K(0)\rangle$	0.001789	0.0027306	0.002742	0.00274273	0.00274273	0.00274273	0.00274273	0.00274273
$\langle K(1)\rangle$	0.0018411	0.0092748	0.0071344	0.0063193	0.004144	0.00274949	0.00274274	0.00274273
$\langle V(0)\rangle$	0.026850	0.0180292	0.0182262	0.018230	0.018230	0.018230	0.018230	0.018230
$\langle V(1)\rangle$	0.026798	0.0114849	0.0138334	0.014534	0.0168287	0.018223	0.018230	0.018230
$\langle H(0)\rangle$	0.0286392	0.0207598	0.0209679	0.0209727	0.0209727	0.0209727	0.0209727	0.0209727
$\langle H(1)\rangle$	0.0286391	0.0207598	0.0209679	0.0209727	0.0209727	0.0209727	0.0209727	0.0209727
$\mathrm{tr}\{\rho^2(0)\}$	0.569338	0.795826	0.79071	0.790569	0.790569	0.790569	0.790569	0.790569
$\mathrm{tr}\{\rho^2(1)\}$	0.569335	0.795825	0.79071	0.790569	0.790569	0.790569	0.790569	0.790569
Err(av)	2.4×10^{-2}	3.7×10^{-2}	2.2×10^{-2}	8.4×10^{-3}	3.1×10^{-3}	6.4×10^{-5}	1.8×10^{-6}	
Err(max)	1.7×10^{-1}	5.1×10^{-1}	4.5×10^{-1}	1.1×10^{-1}	2.6×10^{-2}	4.2×10^{-4}	1.1×10^{-5}	

For each expectation value, results are presented at time $t = 0$ and $t = 1$, corresponding to one cycle of the oscillator. Err(av) is the average error in the elements of ρ with respect to their exact value. Err(max) is the maximum error in the elements of ρ with respect to their exact value.

Table 2(b)
Convergence of the method with respect to extending phase space in the coordinate direction

N	5	8	10	16	20	32	40	
Δx	0.1	0.1	0.1	0.1	0.1	0.1	0.1	
l	.5	.8	1	1.6	2	3.2	4	analytical
$p_{\max}$	10π	10π	10π	10π	10π	10π	10π	
$\mathrm{tr}\{\rho(0)\}$	0.566944	0.7903099	0.883139	0.987906	0.998295	1.	0.999997	1.
$\mathrm{tr}\{\rho(1)\}$	0.566943	0.7903099	0.883139	0.987906	0.998295	1.	0.999997	1.
$\langle K(0)\rangle$	0.0039493	0.0065866	0.0064885	0.003640	0.0029065	0.00274282	0.00274273	0.00274273
$\langle K(1)\rangle$	0.0035682	0.007074	0.011758	0.0051966	0.0033016	0.002743	0.00274273	0.00274273
$\langle V(0)\rangle$	0.00208999	0.0062369	0.0095376	0.0164669	0.017871	0.0182298	0.018230	0.018230
$\langle V(1)\rangle$	0.00247985	0.0057491	0.00485025	0.0149103	0.017476	0.018225	0.018229	0.018230
$\langle H(0)\rangle$	0.060393	0.0128235	0.0160261	0.0201069	0.0207775	0.0209726	0.0209727	0.0209727
$\langle H(1)\rangle$	0.060393	0.0128235	0.0160261	0.0201069	0.0207775	0.0209726	0.0209727	0.0209727
$\mathrm{tr}\{\rho^2(0)\}$	0.304651	0.556046	0.66793	0.782037	0.789763	0.790569	0.790569	0.790569
$\mathrm{tr}\{\rho^2(1)\}$	0.304651	0.556046	0.66793	0.782037	0.789763	0.790569	0.790569	0.790569
Err(av)	3.4×10^{-2}	3.3×10^{-2}	4.1×10^{-2}	9.5×10^{-3}	2.6×10^{-3}	1.1×10^{-5}	1.8×10^{-6}	
Err(max)	5.6×10^{-2}	7.3×10^{-2}	1.2×10^{-1}	2.7×10^{-2}	7.2×10^{-3}	4.2×10^{-5}	1.1×10^{-5}	

Table 2(c)
Results for a minimum volume phase space

N	24	
Δx	0.125	
l	3	analytical
p_{max}	8π	
$\mathrm{tr}\{\rho(0)\}$	0.999996	1.
$\mathrm{tr}\{\rho(1)\}$	0.999997	1.
$\langle K(0)\rangle$	0.00274307	0.00274273
$\langle K(1)\rangle$	0.00274936	0.00274273
$\langle V(0)\rangle$	0.0182288	0.018230
$\langle V(1)\rangle$	0.0182225	0.018230
$\langle H(0)\rangle$	0.0209719	0.0209727
$\langle H(1)\rangle$	0.0209719	0.0209727
$\mathrm{tr}\{\rho^2(0)\}$	0.790567	0.790569
$\mathrm{tr}\{\rho^2(1)\}$	0.790567	0.790569
Err(av)	1.1×10^{-4}	
Err(max)	3.9×10^{-4}	

analytical expectation values according to eq. (4.3). Remembering that care has been taken to converge the time propagation for this table, the conserved quantities maintain their value to the accuracy of the computer. Indeed, $\langle\hat{\rho}(t)\rangle$, $\langle\hat{H}(t)\rangle$ and $\langle\hat{\rho}^2(t)\rangle$ are conserved for all their entries in table 2. Inspecting table 2(a), it is noticed that the initial expectation values are converged for a grid of ten points ($p_{max} = 1.5\pi$ a.u.). However, the propagated expectation values are rather poorly represented for this grid. The convergence of the propagated values occurs for a larger grid of 20 to 32 points ($p_{max} = 6\pi$ a.u. to 8π a.u.). The error analysis of the elements of the density operator leads to the same conclusion regarding the convergence rate as that extracted from the behaviour of the selected expectation values.

In table 2(b), the convergence in phase space with respect to extending the length l of the grid in the coordinate direction is displayed. The maximum momentum has been kept constant at $p_{max} = 10\pi$. Convergence of both initial and final expectation values occurs for a grid size between 20 and 32 points ($l = 2$, a.u. to $l = 3.2$ a.u.). Combining the converged limits of tables 2(a) and 2(b), the minimum volume of phase space has been estimated to be $24h$ [see eq. (3.2)]. This has been explicitly checked by choosing $p_{max} = 8\pi$ a.u. and $l = 3$ a.u. as displayed in table 2(c). Once the volume of phase space is large enough to describe the state of the system at all times, convergence is very fast. This predicted behaviour is clear in table 2.

The convergence in time–energy phase space has been checked by varying the number of Chebychev polynomials in the expansion equation (2.22). The momentum–coordinate phase space has been chosen large enough (40 h) to assure that no errors are introduced due to grid limitations. The same initial state has been propagated for a time of 0.1 cycle, 1 cycle and 5 cycles of the oscillator. Table 3 displays the expectation values and the errors after propagation for the above three times as a function of the number of Chebychev polynomials N_{Ch}. For all times the

Table 3(a)
Convergence of the method with respect to the "time–energy" phase space for $t = 0.1$ oscillator cycles

Et	40	40	40	40	40	40	40	
N_{Ch}	16	39	41	45	48	53	58	analytical
$\mathrm{tr}\{\rho(0.1)\}$	0.06166	0.53871	0.79453	0.975672	0.993284	0.999932	1.	1.
$\langle K(0.1)\rangle$	0.000226	0.00420	0.006278	0.0078571	0.008025	0.0080927	0.0080934	0.0080934
$\langle V(0.1)\rangle$	0.001066	0.0070965	0.010386	0.0126054	0.0128068	0.0128786	0.0128793	0.0128793
$\langle H(0.1)\rangle$	0.00129	0.011298	0.0166635	0.0204625	0.0208319	0.0209713	0.0209727	0.0209727
$\mathrm{tr}\{\rho^2(0.1)\}$	0.000399	0.2066	0.4760	0.747312	0.781132	0.790441	0.790567	0.790569
Err(av)	6.1×10^{-3}	3.5×10^{-3}	1.6×10^{-3}	1.9×10^{-4}	3.4×10^{-5}	6.0×10^{-7}	4.7×10^{-8}	
Err(max)	1.4×10^{-1}	7.0×10^{-2}	3.2×10^{-2}	3.9×10^{-3}	1.1×10^{-3}	1.3×10^{-6}	3.3×10^{-7}	

Table 3(b)
Convergence of the method with respect to the "time–energy" phase space for $t = 1$ oscillator cycles

Et	400	400	400	400	400	400	
N_{Ch}	82	395	405	410	428	436	analytical
$\mathrm{tr}\{\rho(1)\}$	−0.0085	0.35895	0.903563	0.965407	0.99921	1.	1.
$\langle K(1)\rangle$	+0.000145	0.0009144	0.0024396	0.0026234	0.00274228	0.00274274	0.00274274
$\langle V(1)\rangle$	−0.0000033	0.006487	0.0165105	0.0176238	0.0182288	0.01822	0.018230
$\langle H(1)\rangle$	−0.000178	0.007401	0.0189562	0.0202472	0.0209711	0.0209727	0.0209727
$\mathrm{tr}\{\rho^2(1)\}$	0.00024	0.100175	0.648651	0.73874	0.70461	0.790569	0.790569
Err(av)	–	5.0×10^{-3}	7.5×10^{-4}	2.6×10^{-4}	2.2×10^{-6}	1.8×10^{-6}	
Err(max)	–	8.0×10^{-2}	1.2×10^{-2}	4.4×10^{-3}	1.1×10^{-5}	1.1×10^{-5}	

Table 3(c)
Convergence of the method with respect to the "time–energy" phase space for $t = 5$ oscillator cycles

Et	2000	2000	2000	2000	
N_{Ch}	1995	2005	2020	2065	analytical
$\mathrm{tr}\{\rho(5)\}$	0.636346	0.891428	0.988003	1.	1.
$\langle K(5)\rangle$	0.0016077	0.00232	0.00267367	0.00274294	0.00274293
$\langle V(5)\rangle$	0.0117381	0.016367	0.0180474	0.0182298	0.018230
$\langle H(5)\rangle$	0.0133459	0.0186957	0.0207211	0.0209727	0.0209727
$\mathrm{tr}\{\rho^2(5)\}$	0.330158	0.637405	0.774154	0.790569	0.790569
Err(av)	2.7×10^{-3}	3.1×10^{-4}	8.2×10^{-5}	4.6×10^{-6}	
Err(max)	4.6×10^{-2}	1.4×10^{-2}	1.6×10^{-3}	1.8×10^{-5}	

convergence is reached when N_{Ch} is larger than the volume of the time–energy phase space Et, the overhead of the calculation being defined as the number of Chebychev polynomials exceeding Et. This overhead has been termed "tail" in the discussion following eq. (3.3). The shorter the time, the larger the relative overhead becomes. At $t = 0.1$ cycle in table 3 the relative overhead is around 20%, while at $t = 5$ cycles the relative overhead is 3% only. This confirms the statement that the desire for efficiency imposes the usage of long time steps.

It is remarkable that the high accuracy is maintained for a polynomial expansion of a few thousand terms.

5. Splitting of the density operator due to potential scattering: illustrative example

One of the fundamental processes of quantum mechanics is the scattering of a particle due to a collision with a potential. In the example studied, the initial state is localized at the left-hand side of the potential having average momentum directed towards it (figs. 1, 2, $t = 0$). The probability density of the particle is split up by the potential into a transmitted and a reflected part. This simple description already contains the fundamental difficulties of the non-local interpretation of quantum mechanics [62]. In the classical intuitive picture the particle is either reflected or transmitted.

In this section, this process is chosen as a demonstration of a physical process for which a consistent description is only possible by the density operator formalism. Moreover, the method developed in this work allows the direct calculation of the physical quantities involved; in particular, the entropy increase inherent in the irreversible character of the measurement processes. For a detailed description of the many views and controversies concerning this issue, the reader is referred to the book of Jammer [63] and the review paper of Cramer [64]. The formalism used here follows von Neumann [1] and Lindblad [65,66].

In this example a Gaussian potential has been chosen,

$$\hat{V}(x) = V_0 \exp\left[-(x - x_0)^2/2\beta\right], \qquad (5.1)$$

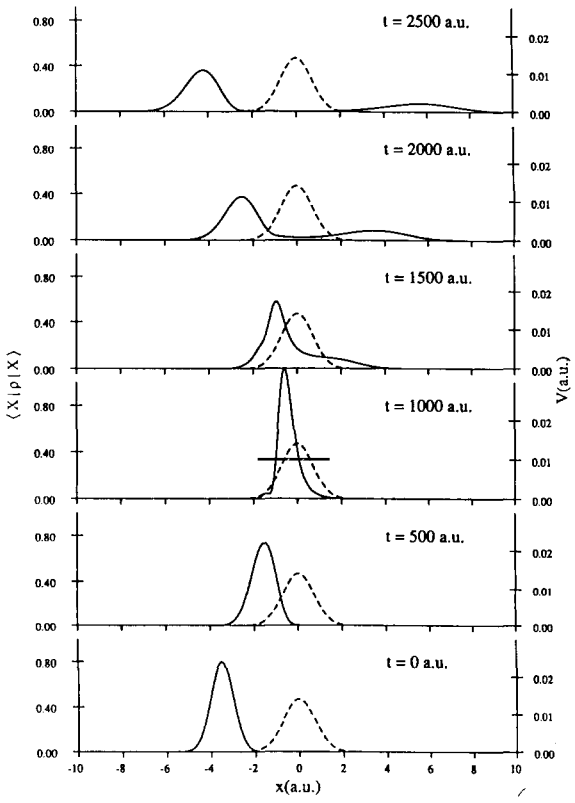

Fig. 1. Reflection and transmission of a Gaussian pure state by a Gaussian potential. Each panel displays a snapshot of the diagonal elements of the density operator in coordinate space (solid line). The potential is drawn by a dashed line.

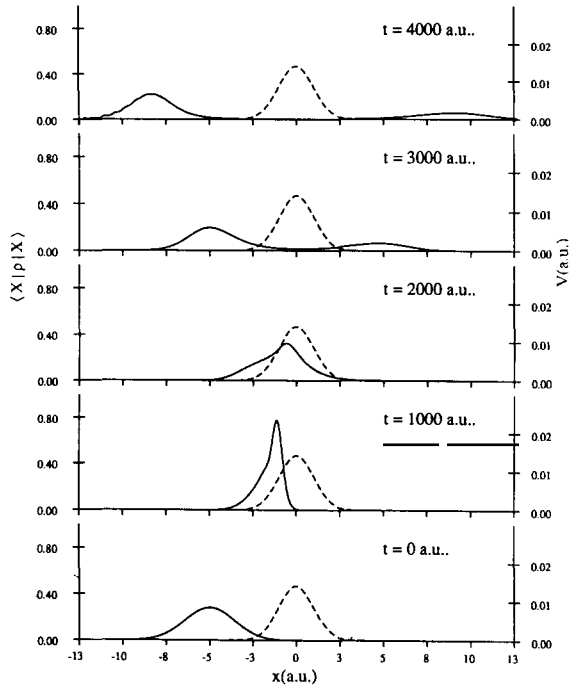

Fig. 2. Reflection and transmission of a Gaussian mixed state by a Gaussian potential. Each panel displays a snapshot of the diagonal elements of the density operator in coordinate space (solid line). The potential is drawn by a dashed line.

where V_0 and β are the strength and range of the potential respectively. The initial density operator has a Gaussian form expressed by eq. (3.6). Both a pure state (fig. 1) and mixed state (fig. 2) have been used as initial conditions. Although the purpose of the calculation is only illustrative, the physical parameters of the system have been chosen to mimic the tunneling process through the potential barrier of the $H + H_2$ reaction. This same model could serve to describe a hydrogen atom diffusing by tunneling on a metal surface [67,68]. Table 4 summarizes the physical parameters used in this example.

The collision process is demonstrated in fig. 1 in which the probability density in coordinate space $\langle x \,|\, \hat{\rho} \,|\, x \rangle$ is displayed for different snap shots. The splitting up of the initial density into an asymptotic transmitted and reflected parts is apparent. This distinction is a physical observable associated with a projection operators

Table 4(a)
Physical parameters for the collision process (pure state)

Physical parameters	
mass	1823 a.u.
Potential:	
V_0	0.0156 a.u.
β	0.5 bohr^{-2}
Grid parameters	
N_x	80
Δx	0.25 a.u.
Δt	500 a.u.
N_{Ch}	46
Initial conditions	
$\langle x(0)\rangle$	−3.5 a.u.
$\langle p(0)\rangle$	7.0 a.u.
$\langle x^2(0)\rangle$	12.501 a.u.
$\langle 1/2(xp(0)+px(0))\rangle$	−24.5 a.u.
$\langle p^2(0)\rangle$	50.0 a.u.
$\langle E\rangle$	0.0137173 a.u.
f	0.251001
tr$\{\rho^2\}$	0.998004

$f = (\langle x^2\rangle - \langle x\rangle^2)(\langle p^2\rangle - \langle p\rangle^2) - (1/2\langle xp + px\rangle - \langle x\rangle\langle p\rangle)^2$

Table 4(b)
Physical parameters for the collision process (mixed state)

Physical parameters	
mass	1823 a.u.
Potential:	
V_0	0.0156 a.u.
β	0.5 bohr^{-2}
Grid parameters	
N_x	100
Δx	0.25 a.u.
Δt	1000 a.u.
N_{Ch}	82
Initial conditions	
$\langle x(0)\rangle$	−5.0 a.u.
$\langle p(0)\rangle$	7.0 a.u.
$\langle x^2(0)\rangle$	27.0 a.u.
$\langle 1/2(xp(0)+px(0))\rangle$	−36.0 a.u.
$\langle p^2(0)\rangle$	50.0 a.u.
$\langle E\rangle$	0.0138533 a.u.
f	1.0
tr$\{\rho^2\}$	0.5

$$\hat{P} = \Theta(x) \tag{5.2}$$

and

$$\hat{Q} = \hat{I} - \hat{P},$$

where Θ is the unit step function. Following von Neumann [1], the state of the system after the above measurement becomes:

$$\hat{\rho}'(t) = \hat{P}\hat{\rho}(t)\hat{P} + \hat{Q}\hat{\rho}(t)\hat{Q}. \tag{5.3}$$

This expression represents the "reduction of the wave packet" assumption which is central to the description of the quantum mechanical measurement processes. The probabilities of the position observables $\hat{P}$ and $\hat{Q}$ describing the particle being to the right or to the left of the potential are respectively:

$$p_R = \mathrm{tr}(\hat{\rho}(t)\hat{P}), \qquad p_L = \mathrm{tr}(\hat{\rho}(t)\hat{Q}), \tag{5.4}$$

the values of which are summarized in table 5 as a function of time. Asymptotic values of p_R and p_L are reached for times longer than 3000 atomic units.

One of the main features of the reduction processes is its irreversibility [1,65]. This fact is demonstrated by the increase of entropy for the reduced state $\hat{\rho}'(t)$ of eq. (5.3), $S(\hat{\rho}') = -\mathrm{tr}\{\hat{\rho}' \ln \hat{\rho}'\}$ displayed as a function of time in table 5. The monotonic increase in $S(\hat{\rho}')$ is clear for both the pure and mixed initial states. This is a numerical confirmation of a fundamental result proved by Lindblad [69]:

$$S(\hat{\rho}'(t)) \geqslant S(\hat{\rho}(t)) = S(\hat{\rho}(0)), \tag{5.5}$$

emphasizing the irreversible nature of the measurement process [1]. The information content of this measurement is given by [70]:

$$I = -(p_R \ln p_R + p_L \ln p_L) \tag{5.6}$$

Other measures of irreversibility may also be calculated directly.

Table 5
Entropies and probabilities of being right or left of the potential barrier as a function of time for a mixed initial state of table 4(b)

t	0	1000	2000	3000	4000
p_R	0.99986	0.99685	0.77499	0.70050	0.70588
p_L	0.00014	0.00315	0.22501	0.29950	0.29412
$S(\rho)$	0.95477	0.95477	0.95478	0.95479	0.95479
$S(\rho')$	0.95521	0.96143	1.20845	1.2321	1.24563
I	0.00138	0.02129	0.53318	0.61044	0.60580

A repeated measurement and therefore a repeated reduction process is one of the routes leading to a semigroup (non-unitary) evolution [71], a subject to be treated in a future paper.

One of the important options built into the density operator formalism is the possibility of selecting only one of the branches of the previous collision as an initial state for a new process. The new normalized initial state takes the form:

$$\hat{\rho}_Q(t) = \frac{\hat{Q}\hat{\rho}(t)\hat{Q}}{\mathrm{tr}(\hat{\rho}(t)\hat{Q})}. \tag{5.8}$$

6. Concluding remarks

The Liouville–von Neumann equation provides a unified description of dynamical and statistical phenomena. In this work it has been demonstrated that a solution to this equation is feasible; therefore, practical modeling of realistic systems is possible. The present method has shown flexibility in the choice of physical parameters such as a change of the potential. In section 4 the accuracy and convergence properties of the method have been investigated. High accuracy has been obtained using a phase-space boundary slightly exceeding the minimum theoretical value, this being an indication of the fast rate of convergence implying efficiency. Efficiency is also obtained by the natural vectorization options provided by the algorithm, in particular, the FFT routines.

An exactly solvable model has been used to check the performance of the method. Convergence in configuration space and convergence in the time propagation have confirmed the theoretical expectations. This pilot study gives the assurance that the algorithm functions correctly.

The method having been established a typical non-trivial example has been chosen, namely, the splitting up of the probability density due to scattering off a potential barrier. In this example it was possible to monitor the branching of an initial non-pure state into transmitted and reflected parts. To summarize, it can be stated that the discrete density operator method has produced a unique environment to explicitly illustrate fundamental phenomena in quantum mechanics.

At this point it is proper to mention a few limitations of the method. Studying the density operator requires twice the dimensionality encountered in wavefunction studies, this feature increasing the numerical effort considerably. Due to the usage of the FFT device, the phase space used has a rectangular shape. One can imagine problems for which the volume in phase space can be reduced by a more elaborate boundary. Moreover, symmetry considerations may dictate the choice of curvilinear coordinates for which an appropriate FFT device has to be designed [73]. Finally, solving a time-dependent problem may be expensive if only asymptotic results, such as in a scattering experiment, are sought. However, insight is gained regarding the instantaneous dynamical mechanism.

In view of the encouraging results of the present study, future possible developments include: the treatment of multi-dimensional problems, open systems possessing dissipation, and explicit time-dependent Liouville superoperators.

The treatment of multi-dimensional systems is an extension of the present work. However, the growth of the computational effort with dimensionality scales as L^{2D} where L is a characteristic length and D is the dimension of configuration space. Inspection of two- and three-dimensional examples may provide a feeling to the extent of these numerical efforts. A one dimensional phase space grid of 32×32 (1024 points) is elevated in a two-dimensional study to 1048576 points, namely, one megaword of computer memory is needed. To date this amount of storage is feasible on most available computers. In three dimensions, sampling phase space reaches the size of 1073741824 points (one gigaword of storage), this being within the limits of currently installed hardware. Extrapolating to four dimensions, storage requirements reach about 1000 gigawords – beyond present-day capabilities. Processing such a vast amount of data requires massive parallel architectures. The FFT algorithm and other parts of the method presented here are extremely suitable to a parallel architectural design. For such algorithms it has been shown [41–43] that the computational duration can be

reduced to $\mathcal{O}(\log N)$ from the sequential scale of $\mathcal{O}(N \log N)$. Currently, the method is being extended to higher dimensions utilizing vector and low-order parallel machines. The ability to treat more dimensions permits the study of collision processes such as elastic scattering, inelastic scattering and reactive collisions. Examples in molecular dynamics include energy transfer among translational, vibrational and rotational degrees of freedom. The new aspect of the present study is the incorporation of mixed states in these processes, a direct stimulation of the experimental situation. The usage of the density operator formalism permits the study of multiple collisions as indicated in section 5.

Dynamics in a condensed phase involves necessarily relaxation and dissipation phenomena. The only consistent treatment is via the density operator formalism, as a pure state evolves into a mixed state in such processes. A detailed study of these aspects is postponed to a future paper [38].

Explicit time dependence may originate from the presence of an external field, the electromagnetic field being an example. Atoms and molecules subject to intense laser radiation have attracted much experimental and theoretical interest. The external field may possess a stochastic component meaning a random variation of its phase and amplitude [72]. Another source of a time-dependent Liouville superoperator results from treating a subset of the degrees of freedom in an approximate fashion. Common examples are classical and semiclassical approximations. Mean field approximations induce time dependence into the generators of the equations of motion. In the framework of mean-field methods algebraic methods [17–19] can be incorporated into a selected part of the degrees of freedom.

Acknowledgements

The Fritz Haber Research Center is supported by the Minerva Gesellschaft für die Forschung, GmbH, München, Germany. R.K. acknowledges support by grants from the US–Israel Binational Science Foundation.

Appendix

The Lagrange coefficients in eq. (3.6) $\lambda_0 - \lambda_5$ as a function of the expectation values $\langle \hat{x} \rangle$, $\langle \hat{p} \rangle$ $\langle \hat{x}^2 \rangle$, $1/2\langle \hat{x}\hat{p} + \hat{p}\hat{x} \rangle$, $\langle \hat{p}^2 \rangle$ are presented.
Define:

$$\beta = \ln\left[\frac{1}{\sqrt{f} - 1} + 1\right], \tag{A.1}$$

where:

$$f = \left(\langle \hat{x}^2 \rangle - \langle \hat{x} \rangle^2\right)\left(\langle \hat{p}^2 \rangle - \langle \hat{p} \rangle^2\right) - \left(\langle \hat{x}\hat{p} - \frac{-\mathrm{i}}{2}\hbar \rangle - \langle \hat{x} \rangle \langle \hat{p} \rangle\right)^2. \tag{A.2}$$

Define:

$$\Delta = \left[\frac{2\hbar^2}{\beta(\mathrm{e}^{\beta} - 1)} + \frac{\hbar^2}{\beta}\right]^{-1}, \tag{A.3}$$

then:

$$\begin{aligned}
\lambda_3 &= -\Delta\left(\langle \hat{p}^2 \rangle - \langle \hat{p} \rangle^2\right), \\
\lambda_4 &= 2\Delta\left(\langle \hat{x}\hat{p} - \frac{\mathrm{i}}{2}\hbar \rangle - \langle \hat{x} \rangle \langle \hat{p} \rangle\right), \\
\lambda_5 &= -\Delta\left(\langle \hat{x}^2 \rangle - \langle \hat{x} \rangle^2\right), \\
\lambda_1 &= -2\lambda_3 \langle \hat{x} \rangle - \lambda_4 \langle \hat{p} \rangle, \\
\lambda_2 &= -2\lambda_5 \langle \hat{p} \rangle - \lambda_4 \langle \hat{x} \rangle.
\end{aligned} \tag{A.4}$$

Equation (3.6) takes the form:

$$\begin{aligned}
\rho(x, x') &= \frac{1}{2\pi} \int \mathrm{d}p \, \exp\left(w_0 + w_1 x + w_2 p + w_3 x^2 + w_4 x p + w_5 p^2\right) \langle x \mid p \rangle \langle p \mid x' \rangle \\
&= \frac{1}{2\pi} \exp\left(w_0 + w_1 x + w_3 x^2\right) \int \mathrm{d}p \\
&\quad \times \exp\left[\left(w_2 + w_4 x + \mathrm{i}x - \mathrm{i}x'\right) p + w_5 p^2\right] \\
&= \frac{1}{2\pi} \exp\left(w_0 + w_1 x + w_3 x^2\right) \left(\frac{\pi}{-w_5}\right)^{1/2} \\
&\quad \times \exp\left(-\frac{\left(2_2 + w_4 x + \mathrm{i}x - \mathrm{i}x'\right)^2}{4w_5}\right),
\end{aligned} \tag{A.5}$$

where the relation:

$$\int e^{ax^2+bx}\,dx = \sqrt{\pi/-a}\; e^{-b^2/4a}, \quad \mathrm{Re}\; a<0,$$

has been used.

w_0–w_5 as a function of λ_0–λ_5 were given by Wilcox [74] and are collected here for completion:

$$\exp\left[\lambda_0+\lambda_1 x+\lambda_2 p+\lambda_3 x^2+\lambda_4 1/2(xp+px)+\lambda_5 p^2\right] = N\left\{\exp\left(w_0+w_1 x+w_2 p-w_3 x^2+w_4 xp+w_5 p^2\right)\right\}, \tag{A.6}$$

$$\begin{aligned}
&\lambda_5^{-1} w_5 = \lambda_3^{-1} w_3 = (\beta J)^{-1}\sinh\beta,\\
&w_4 = c^{-1}(J^{-1}-1),\\
&w_2 = r^2(\tau w_4 + 2\mu w_5),\\
&w_1 = r^2(\mu w_4 + 2\tau w_3).
\end{aligned} \tag{A.7}$$

$$\begin{aligned}
w_0 = {} & \lambda_0 - \tfrac{1}{2}\ln J + r^2(\phi - \lambda_4\lambda_2\lambda_1) + r^4\tau\mu w_4\\
& + r^4\left(4\lambda_5\lambda_3\phi + \beta^2\phi - 8\lambda_5\lambda_3\lambda_4\lambda_2\lambda_1\right)\\
& \times(\beta J)^{-1}\sin\beta,
\end{aligned} \tag{A.8}$$

where

$$J = \cosh\beta - r\lambda_4\sinh\beta, \qquad r = \beta^{-1}c;$$

$$c = [\hat{p},\hat{x}] = -i\hbar,$$

$$\beta = \left[4\lambda_5\lambda_3 - \lambda_4^2\right]^{1/2}, \qquad \phi = \lambda_5\lambda_1^2 + \lambda_3\lambda_2^2,$$

$$\tau = \lambda_4\lambda_2 - 2\lambda_5\lambda_1, \qquad \mu = \lambda_4\lambda_1 - 2\lambda_3\lambda_2.$$

References

[1] J. von Neumann, Mathematical Foundations of Quantum Mechanics (Princeton Univ. Press, Princeton, NJ, 1955).

[2] R. Kubo, J. Phys. Soc. Japan 12 (1957) 570.
M. Toda, R. Kubo and M. Saito, Statistical Physics I, vols. I and II (Springer, Berlin, 1983).

[3] G. Ludwig, Foundation of Quantum Mechanics (Springer, Berlin, 1983).

[4] K. Kraus, States, Effects, and Operations, Lecture Notes in Physics 190 (Springer, Berlin, 1983).

[5] R.C. Tolman, The Principles of Statistical Mechanics (Oxford Univ. Press, Oxford, 1938).

[6] D. ter Haar, Rev. Mod. Phys. 27 (1954) 289.

[7] C. Kittel, Elementary Statistical Physics (Wiley, New York, 1958).

[8] P.A.M. Dirac, Proc. Cambridge Philos. Soc. 26 (1930) 361, 376; 27 (1931) 240.

[9] D. ter Haar, Rep. Prog. Phys. 24 (1961) 304.

[10] U. Fano, Rev. Mod. Phys. 29 (1957) 74.

[11] R. Zwanzig, Phys. Rev. 124 (1961) 983.

[12] D. Forester, Hydrodynamics, Fluctuations, Broken Symmetry and Correlation Functions (Benjamin, Reading, MA, 1975).

[13] A. Abragam, The Principles of Nuclear Magnetism (Clarendon Press, Oxford, 1961).

[14] A. Ben-Reuven and Y. Rabin, Phys. Rev. A 19 (1979) 2056.
Y. Rabin and A. Ben-Reuven, Phys. Rev. A 19 (1979) 1697.

[15] E.T. Jaynes and B. Robertson, in: The Maximum Entropy Formalism, eds. R.D. Levine and M. Tribus (MIT Press, Cambridge, MA, 1979).

[16] Y. Alhassid and R.D. Levine, Phys. Rev. A 18 (1978) 89.

[17] R. Balian and M. Veneroni, Phys. Rev. Lett. 47 (1981) 1355.

[18] N.Z. Tishby and R.D. Levine, Phys. Rev. A 30 (1984) 1477.

[19] R. Balian and M. Veneroni, Ann. Phys. (NY) 164 (1985) 334.

[20] E.A. McCullough and R.E. Wyatt, J. Chem. Phys. 51 (1969) 1253.

[21] P.M. Agrawal and L.M. Raff, J. Chem. Phys. 77 (1982) 3946.

[22] K.C. Kulander, K.R. Sandhya Devi and S.E. Koonin, Phys. Rev. A 25 (1982) 2968.

[23] E.J. Heller, Acc. Chem. Res. 14 (1981) 368.

[24] S. Sawada, R. Heather, B. Jackson and H. Metiu, J. Chem. Phys. 83 (1985) 3009.

[25] M.D. Feit, J.A. Fleck Jr. and A. Steiger, J. Comput. Phys. 47 (1982) 412.

[26] C. Cerjan and R. Kosloff, Phys. Rev. B 34 (1986) 3832.

[27] R.C. Mowrey and D.J. Kouri, Chem. Phys. Lett. 119 (1985) 285.

[28] R.B. Gerber, R. Kosloff and M. Berman, Comput. Phys. Rep. 5 (1986) 59.

[29] T.J. Park and J.C. Light, J. Chem. Phys. 85 (1986) 5870.

[30] R. Kosloff, J. Phys. Chem. 92 (1988) 2087.

[31] V. Mohan and N. Sathyurthy, Comput. Phys. Rep. 7 (1988) 213.

[32] E.B. Davis, Quantum Theory of Open Systems (Academic Press, London, 1976).

[33] G. Lindblad, Commun. Math. Phys. 48 (1976) 119.

[34] V. Gorini, A. Kossakowski and E.C.G. Sudarshan, J. Math. Phys. 17 (1976) 821.

[35] L. Van Hove, Physica 21 (1955) 517; 23 (1957) 441.

[36] U. Fano, in: Lectures on the Many-Body Problem, vol. 11, ed. E.R. Caianello (Academic Press, New York, 1964).

[37] R. Kosloff, Physica A 110 (1982) 346.

[38] M. Berman and R. Kosloff, in preparation.

[39] J.W. Cooley and J.W. Tukey, Math. Comput. 19 (1965) 297.

[40] D. Kosloff and R. Kosloff, J. Comput. Phys. 52 (1983) 35.

[41] M.C. Pease, J. Assoc. Comput. Mach. 15 (1968) 252.

[42] D. Heller, SIAM Rev. 20 (1978) 740.

[43] P.N. Swarztrauber, in: Parallel Computations, ed. G. Rodrigue (Academic Press, New York, 1982).
[44] M. Berman and R.D. Levine, Proc. 1986 Group Theory in Physics Conference Invited Lectures, in: XV Int. Coll. on Group Theoretical Methods in Physics, ed. R. Gilmore (World Scientific, Singapore, 1987) p. 336.
[45] D. Gottlieb and S.A. Orszag, Numerical Analysis of Spectral Methods: Theory and Applications (SIAM, Philadelphia, 1977).
[46] R.N. Bracewell, The Fourier Transform and its Applications, 2nd edn. (McGraw-Hill, New York, 1978).
[47] E.T. Whitaker, Proc. R. Soc. Edinburgh 35 (1915) 181.
[48] H. Nyquist, Trans. AIEE 47 (1928) 617.
[49] C.E. Shannon, Proc. IRE 37 (1949) 10.
[50] J.F. Campbell, Proc. London Math. Soc. 29 (1898) 14.
H.F. Baker, Proc. London Math. Soc. 34 (1902) 347.
F. Hausdorff, Ber. Verhandl. Saechs. Akad. Wiss. Leipzig Math. Naturw. Kl. 58 (1906) 19.
[51] R.L. Burden and J.D. Faires, Numerical Analysis 3rd edn. (PWS Publishers, Boston, MA, 1985).
[52] M. Abramovitz and I.A. Stegan (eds.), Handbook of Mathematical Functions (Dover, New York, 1965).
[53] H. Tal-Ezer and R. Kosloff, J. Chem. Phys. 81 (1984) 3967.
[54] R. Kosloff and H. Tal-Ezer, Chem. Phys. Lett. 127 (1986) 223.
[55] R.J. Glauber, Phys. Rev. 131 (1963) 2766.
[56] S. Mukamel, J. Phys. Chem. 88 (1984) 3185.
[57] C. Temperton, J. Comput. Phys. 52 (1983) 1, 198, 340.
[58] W.H. Louisell, Quantum Statistical Properties of Radiation (Wiley, New York, 1973).
[59] M.C. Pease, Methods of Matrix Algebra (Academic, New York, 1965) p. 321.
[60] A. Messiah, Quantum Mechanics (Wiley, New York, 1958) p. 444, eq. (XII.36 37).
[61] E. Heller J. Chem. Phys. 62 (1975) 1544.
[62] A. Einstein, B. Podolosky and N. Rosen, Phys. Rev. 47 (1935) 777.
[63] M. Jammer, The Philosophy of Quantum Mechanics (Wiley, New York, 1974).
[64] J.G. Cramer, Rev. Mod. Phys. 58 (1986) 647.
[65] G. Lindblad, Commun. Math. Phys. 33 (1973) 305.
[66] R. Kosloff, Adv. Chem. Phys. 46 (1980) 153.
[67] S.C. Wang and R. Gomer, J. Chem. Phys. 83 (1985) 4193.
[68] K.B. Whaley, A. Nitzan and R.B. Gerber, J. Chem. Phys. 84 (1986) 5181.
[69] G. Lindblad, Commun. Math. Phys. 28 (1972) 245.
[70] L. Brillouin, Science and Information Theory (Academic Press, New York, 1956).
[71] K. Kraus, Ann. Phys. 64 (1970) 311.
[72] J.H. Eberly, B.W. Shore and K. Wodkiewicz, Phys. Rev. A 30 (1984) 2381.
[73] R. Bisseling and R. Kosloff, J. Comput. Phys. 59 (1985) 136.
[74] R.M. Wilcox, J. Math. Phys. 8 (1967) 962.